Spin-relaxation mechanisms in InAs quantum well heterostructures

J. D. S. Witt, S. J. Pauka, G. C. Gardner, et al.

View Online   Export Citation   CrossMark

AIP Publishing

Spin-relaxation mechanisms in InAs quantum well heterostructures

View Online   Export Citation   CrossMark

J. D. S. Witt,[1,a)] (iD) S. J. Pauka,[1,2] G. C. Gardner,[3] S. Gronin,[3] T. Wang,[3,4] C. Thomas,[3,4] (iD) M. J. Manfra,[3,4,5] (iD) D. J. Reilly,[1,2] and M. C. Cassidy[2,b)] (iD)

AFFILIATIONS

[1]ARC Centre of Excellence for Engineered Quantum Systems, School of Physics, The University of Sydney, Sydney, NSW 2006, Australia
[2]Microsoft Quantum Sydney, The University of Sydney, Sydney, NSW 2006, Australia
[3]Birck Nanotechnology Center, Purdue University, West Lafayette, Indiana 47907, USA
[4]Department of Physics and Astronomy, Purdue University, West Lafayette, Indiana 47907, USA
[5]Microsoft Quantum Purdue, Purdue University, West Lafayette, Indiana 47907, USA

[a)]Author to whom correspondence should be addressed: jdswitt@gmail.com
[b)]Current address: School of Physics, The University of New South Wales, Sydney, NSW 2052, Australia.

ABSTRACT

Spin–orbit interaction and spin-relaxation mechanisms of a shallow InAs quantum well heterostructure are investigated by magnetoconductance measurements as a function of an applied top-gate voltage. The data are fit using a Iordanskii–Lyanda-Geller–Pikus model and two distinct transport regimes are identified. The spin–orbit interaction splitting energy is extracted from the fits to the data, which also displays two distinct regimes. The different regimes exhibit different spin-scattering mechanisms, the identification of which is of relevance for device platforms of reduced dimensionality which utilize the spin–orbit interaction.

Published under an exclusive license by AIP Publishing. https://doi.org/10.1063/5.0135297

An ability to control and maintain spin-coherence underpins many current technological trends in device physics. Key to optimizing coherence is understanding relaxation. In non-magnetic, low-temperature systems, the spin–orbit interaction (SOI) is one of the dominant effects by which spin-relaxation processes can occur and knowledge of one illuminates the other. The SOI is a relativistic effect which links the electronic translational and spin degrees of freedom. As well as being of fundamental interest—bridging the quantum and the relativistic in a condensed matter system—it holds technological potential, particularly in the field of spintronics, where the ability to electrically manipulate the spin of an electron opens up many new device directions.[1] SOI is also an important constituent in proposals for generating topological states for use in certain qubit schemes.[2,3]

In this paper, we report measurements of the SOI performed on shallow InAs 2DEGs. This is a material which has a non-centrosymmetric zinc blende crystal structure giving it bulk inversion asymmetry (BIA) and the growth within a heterostructure—forming the 2DEG well—adds structural inversion asymmetry (SIA). Both BIA and SIA contribute to the overall SOI of the system. The wells are shallow—10 nm below the sample surface—to enable superconducting

proximitization.[4–11] The measurements reveal two distinct transport regimes, linked to the difference between single- and multi-band occupations of the InAs well. The proportionality relationship between the elastic scattering and spin–orbit lengths within these regimes suggests that the spin-relaxation mechanism differs between them. This has direct implications for spin-coherence in devices of further reduced dimensionality, such as those proposed in hybrid-Majorana schemes. The Dyakonov–Perel' (DP) spin-relaxation mechanism is completely suppressed in one-dimensional systems, whereas the Elliott–Yafet (EY) mechanism is insensitive to the restriction. Understanding these differences is important for the design and operation of future devices utilizing SOI.

The InAs-Al hybrid heterostructure is grown by molecular beam epitaxy using ultra-high purity techniques.[12] The structure includes a quantum well of 5 nm InAs grown on a lower barrier of $In_{0.81}Al_{0.19}As$ at a substrate temperature of 470 C. The top barrier consists of 10 nm of $In_{0.90}Al_{0.10}As$. A 7 nm Al layer is deposited *in situ* after a 2 ML GaAs etch stop is deposited on the semiconductor structure. Hall bar geometries were fabricated using a conventional e-beam lithography process. The mesas were defined using a phosphoric acid etch.

The *in situ* grown aluminum was removed from the patterned Hall bars using a Transene wet-etch. The surface of the samples were then treated with TMA using the pulse–purge function of an ALD tool and a dielectric layer deposited using TMA precursor and H_2O as an oxidizing agent.[13] Finally, metallic top-gates were deposited. Schematics of the Hall bar device and the quantum well heterostructure are shown in the supplementary material. Transport measurements were performed in a dilution refrigerator operating at base temperature ∼10 mK (electron temperature, $T_e \sim 55$ mK) using a standard four-point lock-in technique. The magnetic field was applied perpendicular to the plane of the sample and the magnetoconductance is defined as $\Delta\sigma = \sigma(B) - \sigma(B=0)$.

Magnetoconductance at low magnetic fields is a direct measure of the quantum correction to the classical conductance. This correction arises due to the interference of time-reversed paths, which can either increase or decrease the probability of conduction electrons to be weakly localized and, therefore, decrease or increase the sample conductance. The bounding length-scales of the time-reversed paths are directly related to the intrinsic length-scales of the system. Therefore, the controlled application of magnetic flux (an additional effective length) is the probe with which one can discern the differing contributions of the intrinsic materials parameters. Hence, the electron scattering times within the 2DEG and the effective spin–orbit precession time—which is directly related to the strength of the SOI, can be extracted.

The magnetoconductance data along with fits to the data at several applied top-gate voltages can be seen in Fig. 1. The measurements reveal the presence of both weak localization (WL) and weak antilocalization (WAL) in the devices. There is also a clear evolution of the effects as a function of the applied top-gate voltage. At the most negative applied top gate-voltage [Fig. 1(a)], the low-field peak—associated with WAL—is present alongside the broader inverted peak—indicative
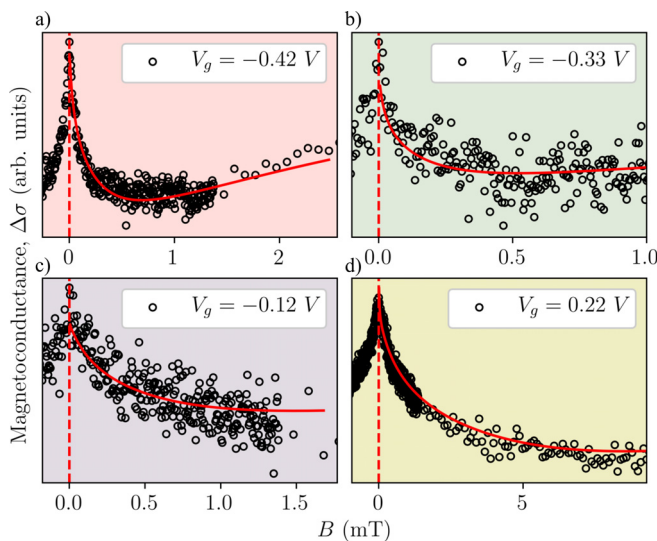
FIG. 1. The magnetoconductance as a function of applied magnetic field are shown. The evolution as a function of the applied top-gate voltage is shown across the four panels (a)–(d). The fits to the data are from the ILP model. The background colors relate the different top-gate voltages to the electron densities in Fig. 2.

of WL. With the increase in the applied top-gate voltage, (b)–(d), the low-field peak remains, but the broader WL dependency is reduced. The main source of experimental error in the measurement is electronic noise on the voltage measurements, which is most apparent when the device resistance is at a minimum, that is, for electron densities which correspond to the highest mobilities.

The Iordanskii–Lyanda-Geller–Pikus (ILP) model was used to fit the magnetoconductance data[14]—it was found not to be possible to achieve a good fit to the magnetoconductance data across the full range of top-gate voltages using the Hikami–Larkin–Nagaoka model. The following definitions were used: the effective electron mass, $m^* = 0.026 m_e$; the electron elastic mean-free-path, $l_e = v_F \tau_e$, where v_F the Fermi velocity and τ_e is the elastic scattering time; the 2D diffusivity, $D = (v_F l_e)/2$; the phase coherence length, $l_\phi = \sqrt{D\tau_\phi}$, where τ_ϕ is the inelastic scattering time; the spin-relaxation rate (in-plane), $1/\tau_{xx} = 2(\Omega_1^2 \tau_e + \Omega_3^2 \tau_{e(3)})$, where Ω_1 and Ω_3 are the linear and cubic precession vectors, respectively, and $\tau_{e(3)}$ is the cubic relaxation time (here, isotropic scattering is assumed, $\tau_e = \tau_{e(3)}$). Representative fits to the magnetoconductance data across the range of applied top-gate voltages are shown in Fig. 1.

The ILP model assumes that the contribution to Ω_1 is from *either* the Rashba *or* Dresselhaus effect, that is, the linear contribution of the other SOI mechanism must be zero. With this assumption, the model is otherwise insensitive to the origin of Ω_1, which is one of the fitting parameters. The other two fitting parameters are Ω_3 and τ_ϕ. The use of this model is justified for the systems under consideration on the assumption that the linear Dresselhaus contribution to the SOI is small, which is typically the case. It is, however, only possible to convincingly fit the data with consideration of both a linear term and a cubic term. For our data, it is also not sufficient to assume a cubic term equivalent to the bulk Dresselhaus value, $\gamma = 26.9$ or $\gamma = 71$ eVÅ^3 (obtained from $\vec{k}\cdot\vec{p}$ and sp_3s^* model calculations, respectively[14])—larger values of γ are required.

From the model, it is possible to extract values for the SOI splitting energy, Δ_{so}, the electron phase coherence length, l_ϕ, and the in-plane spin relaxation length, l_{xx} (the spin–orbit length, $l_{so} = 2l_{xx}$). The electron mean free path l_e was extracted from Hall measurements performed on the same device. These extracted properties display two distinct regimes: a low electron density regime, $n_e < 1.1 \times 10^{12}$ cm^{-2}, and a high electron density regime, $n_e > 1.1 \times 10^{12}$ cm^{-2}. The SOI splitting energy, Δ_{so}, as a function of electron density, n_e, can be seen in the upper panel of Fig. 2. The transition between these two regimes—indicated by a dashed vertical line in Fig. 2—corresponds approximately to an extremum of the gradient of mobility with respect to electron density, which can be seen in the lower panel of Fig. 2. This change is attributed to the onset of the population of the second subband of the well.[15–19] The uncertainty in the values extracted from the fits to the data are greatest in the region of highest mobility where the signal-to-noise ratio in the data is lowest.

The change with electron density of the SOI extends from $\Delta_{so} = 0.55$ meV up to $\Delta_{so} = 4.9$ meV. These values are comparable in magnitude to those observed in InAs quantum wells formed in a number of similar systems.[20–23] Δ_{so} maintaining a constant value in the low electron density regime and increasing linearly in the high electron density regime is consistent with it being a weighted average of the values of the splitting energy of each sub-band and there being a larger intrinsic Δ_{so} in the second sub-band. This lends support to the SOI
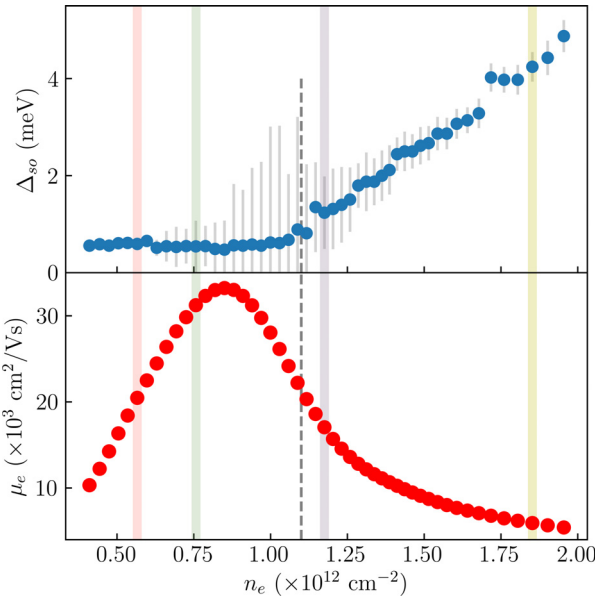
FIG. 2. (Upper panel) The SOI splitting energy extracted from the fits to the magnetoconductance data as a function of the electron density. In the low electron density regime, the errors are smaller than the data plots. (Lower panel) The electron mobility as a function of the electron density, extracted from Hall bar measurements. The dashed gray line indicates what we refer to as the crossover from low- to high-electron density regimes in the text. The color-coded regions correspond to the individual plots in Fig. 1.

FIG. 3. The spin-relaxation length plotted against the electron mean free path. The pink data correspond to the relation of the low electron density single sub-band regime, and the yellow data correspond to the high electron density second sub-band regime. The lines are linear fits to the data shown.

being of a Rashba type—the second mode wavefunction overlaps more strongly with the confining potential than does the first.[24] Band-structure calculations for this material suggest that the filling of the second sub-band—upon application of a sufficiently negative top-gate voltage—is accompanied by a skewing of the well which accumulates electron density nearer to the surface of the heterostructure, which would support this hypothesis.[13] A further possibility behind the increase in Δ_{so} could be the addition of an inter-subband induced spin–orbit term upon transition from a single- to a multiply-occupied sub-band system.[25,26]

The shift in the ratio of WAL to WL with changing electron density can be seen more clearly in the ratio of the values extracted from the fits to the magnetoconductance and from the Hall measurements, and these can be seen in Fig. 3. At low n_e (pink data), the in-plane spin-diffusion length, l_{xx}, falls between the elastic scattering length, l_e, and the phase coherence length, l_ϕ, which allows the formation of both constructive and destructive interference paths. Whereas, at higher n_e (yellow data), the l_{xx} has decreased toward the value of l_e, thereby eliminating the possible destructive paths (necessary for WAL) leaving WL as the dominant effect. These results are consistent with other WAL to WL crossovers observed, which although induced differently, depend ultimately on the ratios of these three lengths.[27–29]

The observed reduction in l_{xx} at higher electron densities would be qualitatively consistent with the electron–electron interaction between the first and second sub-bands leading to a so-called random spin–orbit coupling[30,31]—the skewed second sub-band effectively acting as a near 2D charge impurity layer.[19,32]
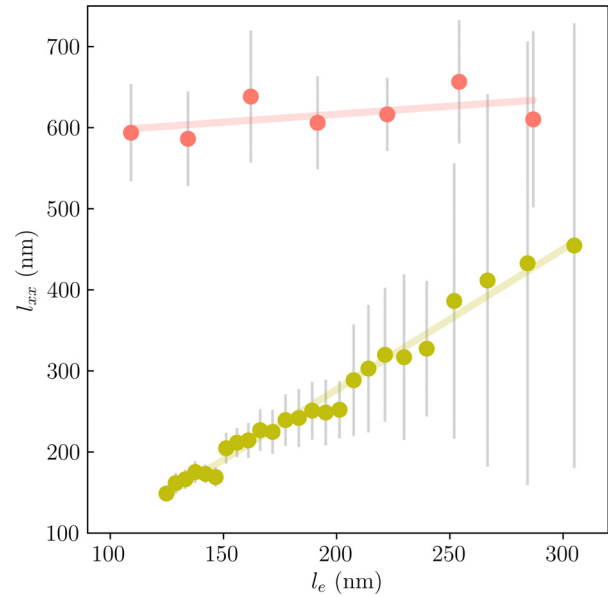
The nature of the spin-relaxation mechanism in the 2DEG manifests in the relation between l_e and l_{xx}. From the data, it is possible to identify two distinct scattering regimes; in the low electron density regime, there is a relatively constant value of l_{xx}, which shows little dependence on l_e, and in the high electron density regime, there is a more definite linear relationship. The longest mean-free path, lowest resistance points have been excluded from this figure—the SNR precludes extracting meaningful values.

In a non-magnetic, (metallic-regime) 2DEG at low-temperature, spin-relaxation can occur via the EY, the DP, and the Bir–Aronov–Pikus (BAP) mechanisms, and the hyperfine interaction (HI). Of these, only the EY and DP mechanisms are of relevance for the devices under consideration here.[33]

The EY mechanism occurs when the electron states are a mixture of spin-up and -down components (mixed due to the SOI coupling between different bands). The ratio of the mixture can change during ordinary momentum scattering (at low temperature from impurities, defects, or boundaries). Spin rotation is, therefore, induced *during* the scattering events and results in a proportional relationship between l_e and l_{xx}.

The DP mechanism arises due to a lack of inversion symmetry— which can be thought of as causing the electron to precess about a succession of differently oriented effective local magnetic fields after each momentum scattering event.[34] There are two limits of operation of this mechanism and, of the two, the more commonly associated with the DP mechanism is the weak limit. In this limit, spin-precession *between* scattering events results in an inverse proportionality relationship between l_e and l_{xx}—the more frequent the momentum scattering the less time the spin has to deflect from its initial value. The DP mechanism in the strong limit—which requires that

$\Delta_{so}\tau_e/\hbar \gg 1$—results in a proportional relationship where $l_{xx} \sim l_e$. In this limit, precession of a substantial angle is able to occur between each momentum scattering event thereby effectively losing the initial spin information *at* each scattering event.

The specific details of the heterostructure clearly bear influence upon the spin-relaxation mechanism in InAs 2DEGs, which has variously been identified as EY[21,35] and DP[27,36–38] experimentally. Also the crossover from one mechanism to the other has been observed as a function of temperature. The data here suggest that the EY mechanism dominates when multiple sub-bands contribute to the electron transport. This seems reasonable in that the second sub-band not only provides an increased opportunity for inter-band scattering—hence the reduction in electron mobility, but also the separately occupied bands will not be degenerate in spin—due to differing strengths of SOI, which leads to increased spin-mixing at scattering events. In the single sub-band limit, the data are less conclusive, but suggestive of a weak DP mechanism being dominant. Based on the values extracted from the fits, the system here does not satisfy the strong DP over the full range of gate-voltages studied. However, $\Delta_{so}\tau_e/\hbar \sim 1$ across this range (taking values from 0.1 to 0.6) not definitively putting the system into either limit.

The phase coherence length is the remaining fitting parameter of the model. The relation between l_ϕ and l_e is approximately proportional across the range of electron densities measured, where the constant of proportionality differs depending on the density regime. In the low electron density regime, $l_\phi/l_e \sim 35$, whereas in the high electron density regime, $l_\phi/l_e \sim 10$. A more detailed comparison of the extracted quantities is shown in the supplementary material. This is qualitatively consistent with the onset of second sub-band filling and the introduction of inter-sub-band scattering[17,19] and increased electron–electron scattering.[31]

The magnetoconductance data support the existence of two top-gate bias accessible sub-band regimes. These regimes experience different spin-relaxation rates and are possessed of differing SOI. The relation of l_e to l_{xx} suggests that EY is the most likely spin-scattering mechanism in the high electron density regime where the occupation of multiple sub-bands which are not degenerate in spin (due to SOI) would lead to increased spin-mixing at scattering events. The single sub-band regime shows little correlation between l_{xx} and l_e, which suggests that the weak DP mechanism may be dominant in this regime. The relation of l_e to l_ϕ has also been discussed, which is a relevant factor for determining whether diffusive or ballistic limits apply in future device structures.[39] We have shown that in controlling the electron mobility and density by applying a top-gate voltage, the strength of the SOI and the spin relaxation mechanisms are also influenced. This interconnectedness offers direct control over the spin coherence within devices, but the spin-relaxation mechanism must also be borne in mind for devices of reduced dimensionality, such as hybrid structures for generating topological phases.

See the supplementary material for further detail of the device measurement setup and the quantum well heterostructure along with a figure directly comparing the extracted length-scales as a function of electron density.

AUTHOR DECLARATIONS
Conflict of Interest

The authors have no conflicts to disclose.

Author Contributions

James D. S. Witt: Conceptualization (lead); Data curation (lead); Formal analysis (lead); Writing – original draft (lead); Writing – review & editing (lead). **Sebastian J. Pauka:** Resources (supporting); Writing – review & editing (supporting). **Geoffrey C. Gardner:** Resources (supporting); Writing – review & editing (supporting). **Sergei Gronin:** Resources (supporting); Writing – review & editing (supporting). **Tian Wang:** Resources (supporting). **Candice Thomas:** Resources (supporting); Writing – review & editing (supporting). **Michael J. Manfra:** Resources (supporting); Writing – review & editing (supporting). **David J. Reilly:** Funding acquisition (lead); Supervision (supporting); Writing – review & editing (supporting). **Maja Cassidy:** Supervision (lead); Writing – review & editing (supporting).

DATA AVAILABILITY

The data that support the findings of this study are available from the corresponding author upon request.

REFERENCES

[1]I. Žutić, J. Fabian, and S. Das Sarma, Rev. Mod. Phys. **76**, 323 (2004).
[2]J. D. Sau, S. Tewari, and S. Das Sarma, Phys. Rev. B **85**, 064512 (2012).
[3]R. M. Lutchyn, E. P. A. M. Bakkers, L. P. Kouwenhoven, P. Krogstrup, C. M. Marcus, and Y. Oreg, Nat. Rev. Mater. **3**, 52 (2018).
[4]W. S. Cole, S. Das Sarma, and T. D. Stanescu, Phys. Rev. B **92**, 174511 (2015).
[5]J. Shabani, M. Kjaergaard, H. J. Suominen, Y. Kim, F. Nichele, K. Pakrouski, T. Stankevic, R. M. Lutchyn, P. Krogstrup, R. Feidenhans'l, S. Kraemer, C. Nayak, M. Troyer, C. M. Marcus, and C. J. Palmstrøm, Phys. Rev. B **93**, 155402 (2016).
[6]H. J. Suominen, M. Kjaergaard, A. R. Hamilton, J. Shabani, C. J. Palmstrøm, C. M. Marcus, and F. Nichele, Phys. Rev. Lett. **119**, 176805 (2017).
[7]L. Casparis, M. R. Connolly, M. Kjaergaard, N. J. Pearson, A. Kringhøj, T. W. Larsen, F. Kuemmeth, T. Wang, C. Thomas, S. Gronin, G. C. Gardner, M. J. Manfra, C. M. Marcus, and K. D. Petersson, Nat. Nanotechnol. **13**, 915 (2018).
[8]W. Mayer, J. Yuan, K. S. Wickramasinghe, T. Nguyen, M. C. Dartiailh, and J. Shabani, Appl. Phys. Lett. **114**, 103104 (2019).
[9]W. Mayer, M. C. Dartiailh, J. Yuan, K. S. Wickramasinghe, E. Rossi, and J. Shabani, Nat. Commun. **11**, 212 (2020).
[10]J. D. S. Witt, G. C. Gardner, C. Thomas, T. Lindemann, S. Gronin, M. J. Manfra, and D. J. Reilly, arXiv:2103.08752 (2021).
[11]A. Jouan, J. D. S. Witt, G. C. Gardner, C. Thomas, T. Lindemann, S. Gronin, M. J. Manfra, and D. J. Reilly, Appl. Phys. Lett. **119**, 172601 (2021).
[12]G. C. Gardner, S. Fallahi, J. D. Watson, and M. J. Manfra, J. Cryst. Growth **441**, 71 (2016).
[13]S. J. Pauka, J. D. S. Witt, C. N. Allen, B. Harlech-Jones, A. Jouan, G. C. Gardner, S. Gronin, T. Wang, C. Thomas, M. J. Manfra, D. J. Reilly, and M. C. Cassidy, J. Appl. Phys. **128**, 114301 (2020).

[14] W. Knap, C. Skierbiszewski, A. Zduniak, E. Litwin-Staszewska, D. Bertho, F. Kobbi, J. L. Robert, G. E. Pikus, F. G. Pikus, S. V. Iordanskii, V. Mosser, K. Zekentes, and Y. B. Lyanda-Geller, Phys. Rev. B **53**, 3912 (1996).

[15] H. Störmer, A. Gossard, and W. Wiegmann, Solid State Commun. **41**, 707 (1982).

[16] R. Fletcher, E. Zaremba, M. D'Iorio, C. T. Foxon, and J. J. Harris, Phys. Rev. B **38**, 7866 (1988).

[17] H. Kroemer, Physica E **20**, 196 (2004).

[18] C. Ellenberger, B. Simovič, R. Leturcq, T. Ihn, S. E. Ulloa, K. Ensslin, D. C. Driscoll, and A. C. Gossard, Phys. Rev. B **74**, 195313 (2006).

[19] T. Tschirky, S. Mueller, C. A. Lehner, S. Fält, T. Ihn, K. Ensslin, and W. Wegscheider, Phys. Rev. B **95**, 115304 (2017).

[20] J. P. Heida, B. J. van Wees, J. J. Kuipers, T. M. Klapwijk, and G. Borghs, Phys. Rev. B **57**, 11911 (1998).

[21] F. Herling, C. Morrison, C. S. Knox, S. Zhang, O. Newell, M. Myronov, E. H. Linfield, and C. H. Marrows, Phys. Rev. B **95**, 155307 (2017).

[22] B. Shojaei, P. J. J. O'Malley, J. Shabani, P. Roushan, B. D. Schultz, R. M. Lutchyn, C. Nayak, J. M. Martinis, and C. J. Palmstrøm, Phys. Rev. B **93**, 075302 (2016).

[23] K. S. Wickramasinghe, W. Mayer, J. Yuan, T. Nguyen, L. Jiao, V. Manucharyan, and J. Shabani, Appl. Phys. Lett. **113**, 262104 (2018).

[24] D. Grundler, Phys. Rev. Lett. **84**, 6074 (2000).

[25] E. Bernardes, J. Schliemann, M. Lee, J. C. Egues, and D. Loss, Phys. Rev. Lett. **99**, 076603 (2007).

[26] R. S. Calsaverini, E. Bernardes, J. C. Egues, and D. Loss, Phys. Rev. B **78**, 155313 (2008).

[27] T. Koga, J. Nitta, T. Akazaki, and H. Takayanagi, Phys. Rev. Lett. **89**, 046801 (2002).

[28] J. B. Miller, D. M. Zumbühl, C. M. Marcus, Y. B. Lyanda-Geller, D. Goldhaber-Gordon, K. Campman, and A. C. Gossard, Phys. Rev. Lett. **90**, 076807 (2003).

[29] V. Sazgari, G. Sullivan, and I. I. Kaya, Phys. Rev. B **101**, 155302 (2020).

[30] J. R. Bindel, M. Pezzotta, J. Ulrich, M. Liebmann, E. Y. Sherman, and M. Morgenstern, Nat. Phys. **12**, 920 (2016).

[31] M. Glazov, E. Sherman, and V. Dugaev, Physica E **42**, 2157 (2010).

[32] S. Das Sarma and E. H. Hwang, Phys. Rev. B **90**, 035425 (2014).

[33] M. Wu, J. Jiang, and M. Weng, Phys. Rep. **493**, 61 (2010).

[34] Unlike an applied magnetic field, these SOI induced effective local magnetic fields do not induce a net polarization.

[35] R. N. Kini, K. Nontapot, G. A. Khodaparast, R. E. Welser, and L. J. Guido, J. Appl. Phys. **103**, 064318 (2008).

[36] J. Luo, H. Munekata, F. F. Fang, and P. J. Stiles, Phys. Rev. B **41**, 7685 (1990).

[37] T. F. Boggess, J. T. Olesberg, C. Yu, M. E. Flatté, and W. H. Lau, Appl. Phys. Lett. **77**, 1333 (2000).

[38] B. N. Murdin, K. Litvinenko, J. Allam, C. R. Pidgeon, M. Bird, K. Morrison, T. Zhang, S. K. Clowes, W. R. Branford, J. Harris, and L. F. Cohen, Phys. Rev. B **72**, 085346 (2005).

[39] A. M. Lobos, R. M. Lutchyn, and S. Das Sarma, Phys. Rev. Lett. **109**, 146403 (2012).